IMA Journal of Numerical Analysis (2000) **20**, 303–332

The planar radiosity equation and its numerical solution

KENDALL ATKINSON
Department of Computer Science and Mathematics, University of Iowa, Iowa City, IA 52242, USA

[Received 7 July 1998 and in revised form 30 January 1999]

This article gives properties of the planar radiosity equation and methods for its numerical solution. Regularity properties of the radiosity solution are examined, including both the effects of corners and the effects of the visibility function. These are taken into account in the design of collocation methods with piecewise polynomial approximating functions. Numerical examples conclude the paper.

Keywords: radiosity equation; integral equation; numerical analysis; collocation methods; Mellin convolution equations; graded mesh methods.

1. Introduction

The radiosity equation is an integral equation which relates the 'radiosity' or 'brightness' at points of a surface to the reflectivity and emissivity at such points, and to the geometric shape of the surface. To better understand the effects of corners and edges on the regularity of the solution function, we first investigate the analogous problem for the planar case. The *planar radiosity equation* is given by

$$u(P) - \rho(P) \int_{\Gamma} u(Q) G(P, Q) V(P, Q)\, \mathrm{d}S_Q = E(P), \qquad P \in \Gamma. \tag{1}$$

Here Γ is a planar curve. It is not necessarily connected, and it is likely to be only piecewise smooth. The emissivity function is $E(P)$, the reflectivity function is $\rho(P)$, and the unknown radiosity function is $u(P)$. It is assumed that $0 \leqslant \rho(P) < 1$ at all points $P \in \Gamma$ (and moreover, that $\|\rho\|_\infty < 1$). The radiosity kernel function G is given by

$$\begin{aligned} G(P, Q) &= \frac{[(P - Q) \cdot \mathbf{n}_P]\big[(Q - P) \cdot \mathbf{n}_Q\big]}{2\,|P - Q|^3} \\ &= \frac{\cos\theta_P \, \cos\theta_Q}{2\,|P - Q|}. \end{aligned} \tag{2}$$

The quantities $\mathbf{n}_P, \mathbf{n}_Q, \theta_P, \theta_Q$ are illustrated in Fig. 1. Later on we say more about $G(P, Q)$. The function $V(P, Q)$ is a 'line of sight' function. More precisely, if the points P and Q can 'see each other' along a straight line segment which does not intersect Γ at any other point, then $V(P, Q) = 1$; otherwise, $V(P, Q) = 0$. An *unoccluded* curve Γ is one for which $V \equiv 1$; otherwise the curve is said to be *occluded*. Physically for occluded curves, 'shadows' occur.

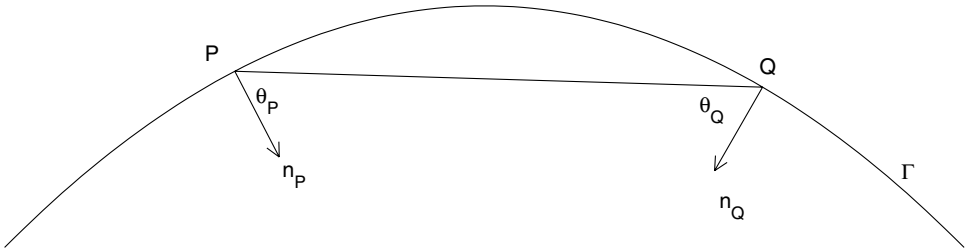

FIG. 1. An illustration of the notation used in defining the radiosity kernel function.

Equation (1) can be obtained as follows. Given Γ, define a cylinder

$$S = \{(x, y, z) \mid (x, y) \in \Gamma,\ -\infty < z < \infty\}$$

and consider the spatial radiosity equation over S. This new equation has the form of (1), but the function $G(P, Q)$ is somewhat different than that given in (2) and the integration is over S. If the spatial radiosity equation is considered over this cylinder, and if the functions E and ρ are independent of z, then the spatial radiosity u is also independent of z. In this situation, the spatial radiosity equation reduces to (1), an integral equation over Γ.

Equation (1) is said to represent the radiosity problem in 'flatland'; but we prefer the interpretation given above, relating it to the spatial equation over a cylindrical surface.

This equation has been studied by a number of authors, as a prelude to studying the spatial radiosity equation. Heckbert (1991, Chapter 3; 1992) gives a very good discussion of the problem, pointing out some of the characteristics of the solution that we also examine later in greater detail. Other important treatments of the determination and use of discontinuities in the radiosity in defining the meshing are given in Lischinski *et al.* (1992) and Cohen & Wallace (1993, §8.5).

Our perspective is somewhat different than in these works, as we are obtaining the properties of the solution by examining the integral equation, relying less on the physical properties of the problem.

For general treatments of the spatial radiosity equation, see Cohen & Wallace (1993) and Sillion & Puech (1994).

The radiosity equation is also studied in the area of thermal radiation within mechanical engineering, and the case we are solving is for opaque, diffuse surfaces with non-participating media. A general treatment of thermal radiation is given by Modest (1993). For a specific example of the radiosity equation in thermal radiation, see Modest (1993, equation (5.3) on p 195).

In §2 we discuss the solvability of the equation, and in §3 we discuss the points of discontinuity of the solution and its derivatives. Because of the great variety of possible curves, we initially deal with a simple case of a polygonal boundary enclosing another polygonal boundary. In §4, we look at the behaviour of the radiosity solution around corner points of the boundary. §5 discusses collocation methods for the solution of equation (1), and §6 gives numerical examples.

2. Solvability of the equation

We first need to consider the solvability of the integral equation (1), which we write abstractly as

$$u - \mathcal{K}u = E \tag{3}$$

with $\mathcal{K}$ an integral operator having the kernel function

$$K(P, Q) = \rho(P)G(P, Q)V(P, Q).$$

Throughout this paper, we consider Γ to be polygonal unless the hypotheses explicitly allow Γ to be more general. Then from (2), it follows easily that $G(P, Q) = 0$ whenever P and Q belong to the same edge of Γ. If P and Q belong to different edges of Γ, there is no difficulty with the existence of the integral in (1), but there is some difficulty as P and Q approach a common corner point of Γ. We discuss the consequences of this in §4. The solvability theory for (3) depends on the following lemma.

LEMMA 1 Assume C is a simple closed piecewise smooth curve, and let $P \in C$ be a point at which a tangent to C exists. Assume the region interior to C is starlike with respect to P. Then

$$\int_C G(P, Q)\, \mathrm{d}S_Q = 1. \tag{4}$$

Proof. The corresponding result for surfaces was shown in Atkinson & Chandler (1998), and therefore we omit the proof of (4). The proof given there was for a convex interior region, but all that is important in that proof is that the region be starlike with respect to the point P. □

A solvability theory for (3) can be developed within the context of $L^\infty(\Gamma)$. There is some initial difficulty in that point evaluation is not considered to be well defined on $L^\infty(\Gamma)$, but this can be handled in the manner discussed in Atkinson *et al.* (1983). The latter shows that point evaluation can be defined as a bounded linear functional which coincides with the normal usage when applied to the evaluation of functions at points at which they are continuous. With this usage, it is straightforward to show that $\mathcal{K}$ is well defined from $L^\infty(\Gamma)$ to $L^\infty(\Gamma)$. Moreover, we obtain

$$\|\mathcal{K}\| \leqslant \|\rho\|_\infty < 1 \tag{5}$$

which is proven as follows.

Assume Γ is polygonal, and let $P \in \Gamma$ be other than a corner point. Let

$$\Gamma_P = \{Q \in \Gamma \mid V(P, Q) = 1\} \cup e_P$$

where e_P is the edge of Γ containing P. By direct examination of (2), $G(P, Q) \geqslant 0$ on Γ_P, with $G(P, Q) \equiv 0$ on e_P. Then for $u \in L^\infty(\Gamma)$,

$$\begin{aligned} |\mathcal{K}u(P)| &= \rho(P) \int_{\Gamma_P} |u(Q)|\, G(P, Q)\, \mathrm{d}S_Q \\ &\leqslant \|u\|_\infty \|\rho\|_\infty \int_{\Gamma_P} G(P, Q)\, \mathrm{d}S_Q. \end{aligned}$$

The result (4) extends to this boundary Γ_P. Assuming Γ_P is not connected, we must extend it to a simple closed polygonal curve $\widetilde{\Gamma}_P$. To do this, pass in a counterclockwise direction about P, viewing Γ_P. As we do so, connect neighbouring endpoints of neighbouring segments of Γ_P using straight line segments. This produces a simple closed polygonal curve $\widetilde{\Gamma}_P$, with all additions to Γ_P visible from P or located on an extension of e_P. Apply Lemma 1 to the curve $\widetilde{\Gamma}_P$, obtaining

$$\int_{\Gamma_P} G(P, Q)\, dS_Q \leqslant \int_{\widetilde{\Gamma}_P} G(P, Q)\, dS_Q = 1.$$

Combining these results proves $\|\mathcal{K}\| \leqslant \|\rho\|_\infty$. The final inequality in (5) follows from the assumption on ρ.

The result (5) is also true for more general piecewise continuous curves Γ, as the above proof needs only a slight modification. The above derivation can also be used to show

$$\int_{\Gamma} G(P, Q)V(P, Q)\, dS_Q \leqslant 1 \tag{6}$$

at all non-corner points $P \in \Gamma$.

The solvability of (3) follows immediately from (5) and the geometric series theorem, with

$$\|u\|_\infty = \left\| (I - \mathcal{K})^{-1} E \right\|_\infty \leqslant \frac{\|E\|_\infty}{1 - \|\mathcal{K}\|}. \tag{7}$$

Moreover, the iteration

$$u_{m+1} = E + \mathcal{K}u_m, \qquad m = 0, 1, \ldots \tag{8}$$

converges to u with

$$\|u - u_m\|_\infty \leqslant \|\mathcal{K}\|^m \|u - u_0\|_\infty, \qquad m \geqslant 0.$$

This iteration is the basis of many commonly used solution methods for solving discretizations of (3).

3. Regularity of the solution

There is a large variety to the possible curves Γ. To make more intuitive our general techniques for analysing these more general boundaries, we initially consider the quite special boundary of Fig. 2. The curve Γ shown in Fig. 2 is composed of inner and outer curves Γ_i and Γ_o, respectively. The subscripts 'o' and 'i' denote 'outer' and 'inner', respectively. We parametrize these two boundaries by $r_o(s)$ and $r_i(s)$, respectively, with $0 \leqslant s \leqslant 1$. It is assumed that s will be directly proportional to the arc-length on each boundary, so that $|r_o'(t)|$ and $|r_i'(t)|$ are constant (except at the corner points, where they are undefined), and these constants are denoted respectively by $|r_o'|$ and $|r_i'|$. In Fig. 2, the corners of Γ_o have coordinates $\{(\pm 1, \pm 1)\}$, those of Γ_i have coordinates $\{(\pm a, \pm a)\}$ for some $0 < a < 1$. Certain important points on the boundary are marked with special symbols for easy reference, and their significance is explained below.

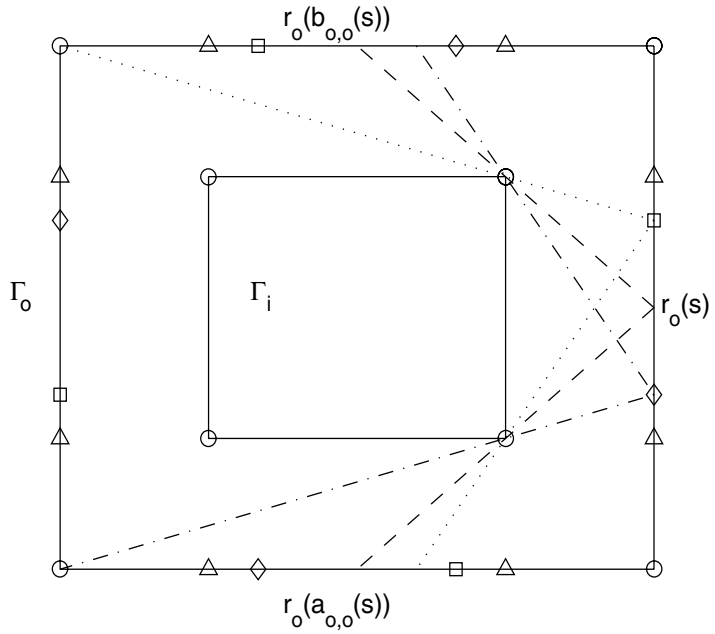

FIG. 2. The points △ are discontinuities of $a_{o,i}(s)$ and $b_{o,i}(s)$; the points △ and □ are discontinuities of $b'_{o,o}(s)$, and the points △ and ◇ are discontinuities of $a'_{o,o}(t)$.

Define the parametrization of the outer boundary Γ_o as follows. For $0 \leqslant s \leqslant 1$,

$$r_o(s) = \begin{cases} x = 1 - 8s, & y = 1, & 0 \leqslant s \leqslant \frac{1}{4}, \\ x = -1, & y = 1 - 8\left(s - \frac{1}{4}\right), & \frac{1}{4} \leqslant s \leqslant \frac{1}{2}, \\ x = -1 + 8\left(s - \frac{1}{2}\right), & y = -1, & \frac{1}{2} \leqslant s \leqslant \frac{3}{4}, \\ x = 1, & y = -1 + 8\left(s - \frac{3}{4}\right), & \frac{3}{4} \leqslant s \leqslant 1. \end{cases}$$

Extend $r_o(s)$ periodically to $-\infty < s < \infty$ using

$$r_o(s + k) = r_o(s), \qquad 0 \leqslant s \leqslant 1, \quad k \in \mathbb{Z}.$$

Define the parametrization of the inner boundary Γ_i using

$$r_i(s) = a\, r_o(1 - s), \qquad -\infty < s < \infty.$$

This means the outer boundary is oriented counterclockwise and the inner boundary is oriented clockwise. Note that both $r'_o(s)$ and $r'_i(s)$ are piecewise continuous, lacking continuity only at the corners of the respective curves Γ_o and Γ_i. For more general two-part curves, such as those in Figs 3 and 4, we can also define analogous parametrizations.

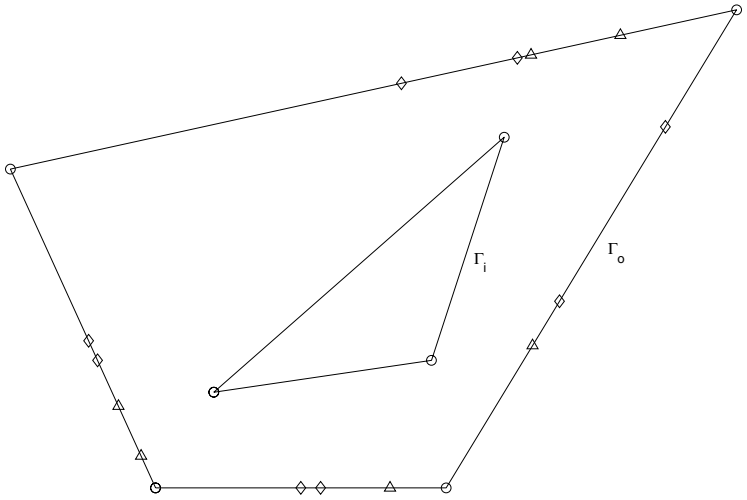

FIG. 3. The points marked '$\circ$', '$\diamond$', and '$\triangle$' are locations at which the derivative u' with respect to the arc-length is likely to be discontinuous.

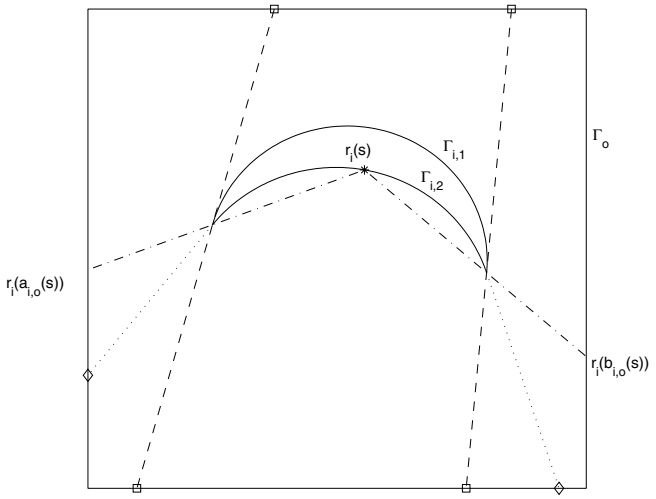

FIG. 4. The outer boundary is the unit square; the inner boundary is a crescent. The symbols '$\diamond$' and '$\square$' denote some points at which u' is usually discontinuous.

The results of this section are derived only for the polygonal-type boundaries of Figs 2 and 3. Later in the section, we discuss the generalization of these results to curved piecewise smooth boundaries (e.g. Fig. 4) and to more complicated boundaries, polygonal and otherwise.

For the radiosity equation (1), we have the following for the unknown solution u on the outer boundary of Fig. 2 (and similarly for Figs 3 and 4). For $0 \leqslant s \leqslant 1$,

$$\begin{aligned} u(r_o(s)) &= E(r_o(s)) + \rho(r_o(s)) \int_{a_{o,o}(s)}^{b_{o,o}(s)} G(r_o(s), r_o(t)) u(r_o(t)) \left|r_o'\right| \mathrm{d}t \\ &\quad + \rho(r_o(s)) \int_{a_{o,i}(s)}^{b_{o,i}(s)} G(r_o(s), r_i(t)) u(r_i(t)) \left|r_i'\right| \mathrm{d}t \\ &\equiv E(r_o(s)) + \rho(r_o(s)) \left[I_1(s) + I_2(s)\right]. \end{aligned} \tag{9}$$

The functions $\left\{a_{o,o}(s), b_{o,o}(s)\right\}$ are the limits on t such that $r_o(t) \in \Gamma_o$ can be seen by $r_o(s)$; and $\left\{a_{o,i}(s), b_{o,i}(s)\right\}$ are the limits on t such that $r_i(t) \in \Gamma_i$ can be seen by $r_o(s)$. Figure 2 contains an example in which the points $r_o\left(b_{o,o}(s)\right)$, $r_o\left(a_{o,o}(s)\right)$ are shown for a generic point $r_o(s)$ on the right-hand side of Γ_o. The functions $\left\{a_{o,o}(s),\ b_{o,o}(s)\right\}$ vary continuously with s, but the derivative is discontinuous at certain critical points in addition to the corners of the outer boundary. For these additional critical points, see the points marked '$\diamond$', '$\square$', and '$\triangle$'. The asserted discontinuous behaviour can be shown directly by giving formulas for $\left\{a_{o,o}(s),\ b_{o,o}(s)\right\}$; it can also be argued from more general principles.

The function $a_{o,o}'(s)$ is discontinuous at the points '$\diamond$', as the point $r_o\left(a_{o,o}(s)\right)$ is a corner point in such cases. Analogously, the function $b_{o,o}'(s)$ is discontinuous at the points '$\square$', as $r_o\left(b_{o,o}(s)\right)$ is then a corner point. The points marked '$\triangle$' are the intersections of the lines containing the edges of the inner boundary Γ_i with the outer boundary Γ_o. At such points, the functions $a_{o,o}'(s)$ and $b_{o,o}'(s)$ are discontinuous due to the 'line of sight segment' from $r_o(s)$ to $r_o\left(a_{o,o}(s)\right)$ changing from pivoting about one corner of Γ_i to another corner of Γ_i as s increases.

Considering the final integral $I_2(s)$ in (9), the limits $\left\{a_{o,i}(s), b_{o,i}(s)\right\}$ are piecewise constant functions; the discontinuities s again correspond to the points $r_o(s)$ on Γ_o that are marked '$\triangle$'. However, the last integral in (9) is not discontinuous for such values of s, a result we justify later.

For the radiosity equation viewed from a point $r_i(s)$ on the inner boundary Γ_i,

$$u(r_i(s)) = E(r_i(s)) + \rho(r_i(s)) \int_{a_{i,o}(s)}^{b_{i,o}(s)} G(r_i(s), r_o(t)) u(r_o(t)) \left|r_o'\right| \mathrm{d}t. \tag{10}$$

The functions $\left\{a_{i,o}(s), b_{i,o}(s)\right\}$ are the limits on t for the integration over Γ_o. Note that $\left\{a_{i,o}(s), b_{i,o}(s)\right\}$ are piecewise constant functions and they are discontinuous at points s corresponding to $r_i(s)$ a corner of the inner boundary Γ_i.

3.1 *Continuity of the solution*

We assume the given data functions ρ and E are continuous except at corners of Γ. From this and (9)–(10), we show $u(P)$ is continuous except possibly at the corner points of Γ. Examining first the continuity of $u(r_o(s))$ by means of (9), the continuity of $\left\{a_{o,o}(s), b_{o,o}(s)\right\}$ leads to continuity for the first integral $I_1(s)$ on the right-hand side of (9) at all non-corner points $r_o(s)$. The special case that $r_o(s)$ is a corner point of Γ_o is examined later in §4 (cf (24)); for $u(P)$ continuous at the corner, so is $I_1(s)$.

For the second integral $I_2(s)$ on the right-hand side of (9), we must examine what happens as the point $r_0(s)$ passes through a corner point of Γ_o and through any point marked '$\triangle$', as $\{a_{o,i}(s), b_{o,i}(s)\}$ are discontinuous at such points. For the discussion of the continuity of $I_2(s)$, we begin with the corner points of Γ_o. As $P = r_o(s)$ passes through a corner of Γ_o, the normal $\mathbf{n}_P$ changes direction, discontinuously. As a consequence, the kernel function $G(P, Q)$ also changes discontinuously at all points $Q \in \Gamma_i$. It is then straightforward to show that $I_2(s)$ is usually discontinuous at the corner points of Γ_o, making $u(r_o(s))$ also discontinuous at such points. This is illustrated later in §6.

Consider next the continuity of $I_2(s)$ at the points marked '$\triangle$'. Let a point $\triangle$ be given by $r_0(s^*)$, and assume that for $s < s^*$ and $s^* - s$ small, one can see only a single edge e_1 of Γ_i; for $s > s^*$ and $s - s^*$ small, one can see both e_1 and a second edge e_2. Then

$$\int_{a_{o,i}(s)}^{b_{o,i}(s)} G(r_o(s), r_i(t))u(r_i(t))\,\mathrm{d}t = \begin{cases} \displaystyle\int_{e_1} G(r_o(s), Q)u(Q)\,\mathrm{d}S_Q, & s < s^*, \\ \displaystyle\int_{e_1 \cup e_2} G(r_o(s), Q)u(Q)\,\mathrm{d}S_Q, & s > s^*. \end{cases}$$

We must show that

$$\lim_{s \searrow s^*} \int_{e_2} G(r_o(s), Q)u(Q)\,\mathrm{d}S_Q = 0. \tag{11}$$

This follows by examining the kernel function $G(r_o(s), Q)$ of (2). From there, as $s \searrow s^*$, the line $r_o(s) - Q$ becomes perpendicular to $\mathbf{n}_Q$, and thus the kernel approaches 0, proving (11). Note that this proof works as well for the polygonal curves of Figs 3 and 5 as it does for Fig. 2. This also completes the proof of the continuity of $u(r_o(s))$.

To discuss whether $u(r_i(s))$ is continuous, consider (10). Away from a corner of Γ_i, the integration in (10) is a simple integration of a nonsingular kernel function $G(r_i(s), Q)$ and a bounded measurable function $u(Q)$ over a fixed portion of Γ_o. It follows that $u(r_i(s))$ is continuous away from corners of Γ_i. A discontinuity of $u(r_i(s))$ follows at any corner of Γ_i at which either ρ and E is discontinuous. But even if ρ and E are continuous at the corners of Γ, it is likely that the integral in (10) is discontinuous and that therefore $u(r_i(s))$ is also discontinuous. The reason for the discontinuity in the integral is that as one travels along Γ_i and around a corner, the portion of Γ_o that is viewable changes significantly, and therefore the integral of

$$G(r_i(s), r_o(t))u(r_o(t))$$

also changes. It is very unlikely that the integral will remain the same as $r_i(s)$ passes through such a corner of Γ_i (except for cases when $u(r_o(t))$ possesses certain symmetry relative to the corner). This will happen at any corner at which the angle facing into the region is greater than π radians. In the much more complicated Fig. 5 this happens with corners on both the interior and exterior boundaries.

In general, these results extend easily to any polygonal curve contained within the interior of another polygonal curve. To generalize this result on the continuity of u to nonpolygonal curves such as Fig. 4 requires some additional discussion, but it is a fairly straightforward analogue of what has been discussed for Fig. 2. An important lemma for doing such is the following.

LEMMA 2 Assume C to be a twice continuously differential curve (open or closed) and let $P, Q \in C$. Then

$$|G(P, Q)| \leqslant \alpha_C \, |P - Q|$$

with α_C dependent on C.

Proof. The proof is an immediate consequence of

$$\left|\cos\theta_Q\right|, |\cos\theta_P| \leqslant \beta_C \, |P - Q|, \quad P, Q \in C.$$

A proof of this can be found in most books on boundary integral equation reformulations of Laplace's equation in the plane. In addition,

$$\frac{\cos\theta_Q}{2\,|P - Q|}$$

is a continuous function of P, Q on C, with a removable singularity at $P = Q$, and it is the double-layer kernel obtained when writing a solution of Laplace's equation as a double-layer potential. □

3.2 *Continuity of the first derivative*

We investigate the behaviour of the derivative of the unknown with respect to s, which is a constant multiple of the arc-length. To this end, form the derivative of formulas (9)–(10) with respect to s, doing so at points other than the corner points of Γ.

$$\begin{aligned}
\frac{\mathrm{d}}{\mathrm{d}s}u(r_o(s)) = {} & [E(r_o(s))]' + \rho(r_o(s)) \int_{a_{o,o}(s)}^{b_{o,o}(s)} \frac{\mathrm{d}}{\mathrm{d}s}\left[G(r_o(s), r_o(t))\right] u(r_o(t)) \left|r_o'\right| \, \mathrm{d}t \\
& + [\rho(r_o(s))]' \int_{a_{o,o}(s)}^{b_{o,o}(s)} G(r_o(s), r_o(t)) u(r_o(t)) \left|r_o'\right| \, \mathrm{d}t \\
& + \rho(r_o(s)) G\left(r_o(s), r_o(b_{o,o}(s))\right) u\left(r_o(b_{o,o}(s))\right) \left|r_o'\right| b_{o,o}'(s) \\
& - \rho(r_o(s)) G\left(r_o(s), r_o(a_{o,o}(s))\right) u\left(r_o(a_{o,o}(s))\right) \left|r_o'\right| a_{o,o}'(s) \\
& + \rho(r_o(s)) \int_{a_{o,i}(s)}^{b_{o,i}(s)} \frac{\mathrm{d}}{\mathrm{d}s}\left[G(r_o(s), r_i(t))\right] u(r_i(t)) \left|r_i'\right| \, \mathrm{d}t \\
& + [\rho(r_o(s))]' \int_{a_{o,i}(s)}^{b_{o,i}(s)} G(r_o(s), r_i(t)) u(r_i(t)) \left|r_i'\right| \, \mathrm{d}t \\
\equiv {} & [E(r_o(s))]' + I_1 + I_2 + I_3 + I_4 + I_5 + I_6.
\end{aligned} \tag{12}$$

$$\begin{aligned}
\frac{\mathrm{d}}{\mathrm{d}s}u(r_i(s)) = {} & [E(r_i(s))]' + \rho(r_i(s)) \int_{a_{i,o}(s)}^{b_{i,o}(s)} \frac{\mathrm{d}}{\mathrm{d}s}\left[G(r_i(s), r_o(t))\right] u(r_o(t)) \left|r_o'\right| \, \mathrm{d}t \\
& + [\rho(r_i(s))]' \int_{a_{i,o}(s)}^{b_{i,o}(s)} G(r_i(s), r_o(t)) u(r_o(t)) \left|r_o'\right| \, \mathrm{d}t \\
\equiv {} & [E(r_i(s))]' + I_7 + I_8.
\end{aligned} \tag{13}$$

The integrals $I_1, ..., I_8$ are assigned based on the order given in the formulas containing the integrals.

The above formulas contain the first derivatives of $E(r(s))$ and $\rho(r(s))$. We initially assume for this section that these derivatives are continuous except possibly at points at which we expect $u(r(s))$ to be discontinuous, namely the corners of Γ. Referring to Fig. 2, it will turn out that some of the remaining terms in the above formulas are likely to be discontinuous at the additional points denoted '$\diamond$', '$\square$', and '$\triangle$'. Therefore, it would not change the differentiability results to also allow the derivatives $[E(r(s))]'$ and $[\rho(r(s))]'$ to be discontinuous at those same points.

Examine the regularity of $[u(r_o(s))]'$ by using (12), with $r_o(s)$ not a corner point. For terms I_2 and I_6, the only points of possible discontinuity are the corner points of Γ_o. For I_1, the integrand is identically zero for $r_o(s)$ and $r_o(t)$ sharing a common edge, and therefore the integrand is not singular, making I_1 a continuous function of s away from the corners of Γ_o. The integral I_5 has an integrand that is well defined except for the corners of Γ, and it is nonsingular at all other points, along with all orders of derivatives of it.

The remaining terms are I_3 and I_4, and they are discontinuous at some new points of the boundary, namely where $a'_{o,o}(s)$ and $b'_{o,o}(s)$ are discontinuous. Thus in Fig. 2, the derivative $[u(r_o(s))]'$ is likely to be discontinuous at the corner points and at the points denoted '$\diamond$', '$\square$', and '$\triangle$'

The terms in (13) are all well behaved except at the corners of Γ_i. This follows from the function $G(r_i(s), r_o(t))$ being a well behaved function of s and t except for $r_i(s)$ a corner point of Γ_i. Thus $[u(r_i(s))]'$ is continuous except possibly at the corners of Γ_i, and it is likely to be discontinuous at those corners.

These results for the integral limits and for the continuity of the function $u(r(s))$ and its derivative generalize immediately to boundaries Γ consisting of an inner polygon Γ_i and an outer polygon Γ_o with both polygons having convex interiors. Thus in Fig. 3, the first derivative $[u(r(s))]'$ is likely to be discontinuous at the corner points and at the points denoted '$\diamond$' and '$\triangle$'; generalizing further, in Fig. 5 $[u(r(s))]'$ is likely to be discontinuous at the corner points and at the points denoted '$\diamond$'.

The points marked '$\diamond$' and '$\square$' of Fig. 2 and the points marked '$\diamond$' in Fig. 3 are obtained by connecting corners of Γ_i to corners of Γ_o, finding where they intersect on Γ_o, provided the line segment involved is located entirely within the region between Γ_i and Γ_o. The points marked '$\triangle$' are obtained by extending line segments of Γ_i to where they intersect with Γ_o, again provided the extended line segment is located entirely within the region between Γ_i and Γ_o. We can also have the situation of line segments of Γ_o being extended to have an intersection with some point of Γ_i, with a behaviour for $u(r(s))$ analogous to that for points '$\triangle$' on Γ_o of Figs 2 and 3. An example of the latter is shown in Fig. 5, in which both Γ_i and Γ_o are more complicated than in the earlier cases.

3.3 *Continuity of the second derivative*

In order to avoid problems involved with analysing the second derivative of $\mathcal{K}u$, we use iteration to re-write the equation $u = E + \mathcal{K}u$ as

$$u = E + \mathcal{K}E + \mathcal{K}^2 u. \tag{14}$$

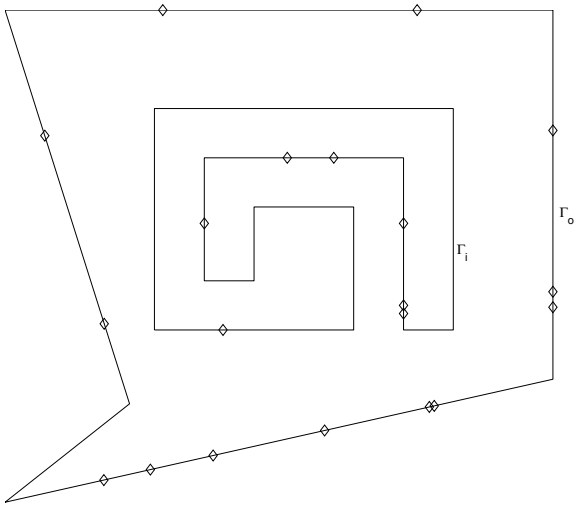

FIG. 5. Points at which the first derivative is likely to be discontinuous are marked '$\diamond$', in addition to the corner points.

We begin by considering the second derivative of $\mathcal{K}E$, and then we consider the second derivative of $\mathcal{K}^2 u$. In analogy with (9) and (10), we have

$$\begin{aligned}\mathcal{K}E\,(r_o(s)) = \rho(r_o(s))\int_{a_{o,o}(s)}^{b_{o,o}(s)} G(r_o(s), r_o(t))E(r_o(t))\left|r_o'\right|\,\mathrm{d}t \\ +\rho(r_o(s))\int_{a_{o,i}(s)}^{b_{o,i}(s)} G(r_o(s), r_i(t))E(r_i(t))\left|r_i'\right|\,\mathrm{d}t.\end{aligned} \tag{15}$$

$$\mathcal{K}E(r_i(s)) = \rho(r_i(s))\int_{a_{i,o}(s)}^{b_{i,o}(s)} G(r_i(s), r_o(t))E(r_o(t))\left|r_o'\right|\,\mathrm{d}t. \tag{16}$$

In analogy with the discussion of (13), the derivative of (16) presents no problems, with the points of difficulty being again the four corners of Γ_i, and nothing else. For the second derivative, we can proceed exactly as for the first derivative. Again there is no difficulty for $r_i(s)$ not a corner point of Γ_i, as the integrand is nonsingular. The derivative of (15) is analogous to that of (12), with u replaced by E. For the second derivative, all terms are well behaved away from the points previously identified as points of possible discontinuity for u and its first derivative.

The more interesting case is that of the second derivative of $\mathcal{K}^2 u$. On the outer boundary,

$$
\begin{aligned}
&\left(\mathcal{K}^2 u\right)(r_o(s)) \\
&= \left|r_o'\right|^2 \rho(r_o(s)) \int_{a_{o,o}(s)}^{b_{o,o}(s)} G(r_o(s), r_o(\tau))\rho(r_o(\tau)) \int_{a_{o,o}(\tau)}^{b_{o,o}(\tau)} G(r_o(\tau), r_o(t))u(r_o(t))\,\mathrm{d}t\,\mathrm{d}\tau \\
&+ \left|r_o'\right|\left|r_i'\right| \rho(r_o(s)) \int_{a_{o,o}(s)}^{b_{o,o}(s)} G(r_o(s), r_o(\tau))\rho(r_o(\tau)) \int_{a_{o,i}(\tau)}^{b_{o,i}(\tau)} G(r_o(\tau), r_i(t))u(r_i(t))\,\mathrm{d}t\,\mathrm{d}\tau \\
&+ \left|r_o'\right|\left|r_i'\right| \rho(r_o(s)) \int_{a_{o,i}(s)}^{b_{o,i}(s)} G(r_o(s), r_i(\tau))\rho(r_i(\tau)) \int_{a_{i,o}(\tau)}^{b_{i,o}(\tau)} G(r_i(\tau), r_o(t))u(r_o(t))\,\mathrm{d}t\,\mathrm{d}\tau.
\end{aligned}
\tag{17}
$$

On the inner boundary,

$$
\begin{aligned}
&\left(\mathcal{K}^2 u\right)(r_i(s)) \\
&= \left|r_o'\right|^2 \rho(r_i(s)) \int_{a_{i,o}(s)}^{b_{i,o}(s)} G(r_i(s), r_o(\tau))\rho(r_o(\tau)) \int_{a_{o,o}(\tau)}^{b_{o,o}(\tau)} G(r_o(\tau), r_o(t))u(r_o(t))\,\mathrm{d}t\,\mathrm{d}\tau \\
&+ \left|r_o'\right|\left|r_i'\right| \rho(r_i(s)) \int_{a_{i,o}(s)}^{b_{i,o}(s)} G(r_i(s), r_o(\tau))\rho(r_o(\tau)) \int_{a_{o,i}(\tau)}^{b_{o,i}(\tau)} G(r_o(\tau), r_i(t))u(r_i(t))\,\mathrm{d}t\,\mathrm{d}\tau.
\end{aligned}
\tag{18}
$$

The second derivative will be complicated, but there are only a few terms in which new points of possible bad behaviour are introduced. The most important parts in the first derivative include the term

$$
\int_{a_{o,o}(b_{o,o}(s))}^{b_{o,o}(b_{o,o}(s))} G(r_o(b_{o,o}(s)), r_o(t))u(r_o(t))\,\mathrm{d}t
$$

and the corresponding term obtained by reversing the roles of $a_{o,o}$ and $b_{o,o}$. In forming the various derivatives, recall that the functions

$$
\left\{a_{o,i}(s), b_{o,i}(s), a_{i,o}(s), b_{i,o}(s)\right\}
$$

are piecewise constant. When taking the second derivative in the above expression, the important new expressions are

$$
\begin{gathered}
\frac{\mathrm{d}}{\mathrm{d}s} b_{o,o}(b_{o,o}(s)),\ \frac{\mathrm{d}}{\mathrm{d}s} a_{o,o}(b_{o,o}(s)), \\
G(r_o(b_{o,o}(s)), r_o(b_{o,o}(b_{o,o}(s))))\, u(r_o(b_{o,o}(b_{o,o}(s)))), \\
G(r_o(b_{o,o}(s)), r_o(a_{o,o}(b_{o,o}(s))))\, u(r_o(a_{o,o}(b_{o,o}(s))))
\end{gathered}
\tag{19}
$$

and the corresponding expressions in which the roles of $b_{o,o}$ and $a_{o,o}$ are reversed. Thus we must look at the points based on 'iterating' the previous points of potential bad behaviour:

$$
r_o(b_{o,o}(b_{o,o}(s))),\ r_o(a_{o,o}(b_{o,o}(s))),\ r_o(b_{o,o}(a_{o,o}(s))),\ r_o(a_{o,o}(a_{o,o}(s))).
$$

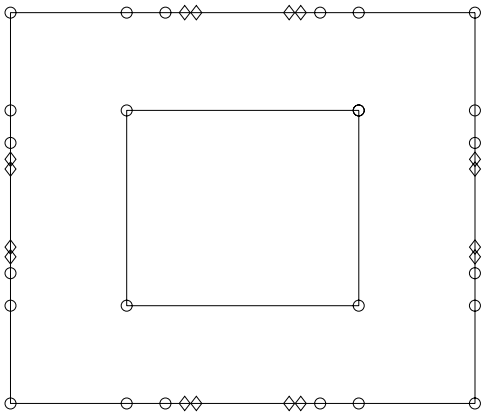

FIG. 6. The points at which $a_{o,o} \circ a_{o,o}$ and $b_{o,o} \circ b_{o,o}$ are ill behaved are indicated by '$\diamond$'; the original points of ill behaviour for $a_{o,o}$ and $b_{o,o}$ are indicated by '$\circ$', namely the elements of $\mathcal{S}_1$.

The quantities $a_{o,o}(b_{o,o}(s))$ and $b_{o,o}(a_{o,o}(s))$ are not of interest, as

$$a_{o,o}(b_{o,o}(s)) = s, \qquad b_{o,o}(a_{o,o}(s)) = s, \qquad 0 \leqslant s \leqslant 1 \tag{20}$$

and thus

$$r_o(a_{o,o}(b_{o,o}(s))) \equiv r_o(b_{o,o}(a_{o,o}(s))) \equiv r_o(s).$$

The truth of (20) is immediate from a picture such as Fig. 2, as it says that, when travelling a straight line, what is the upper limit when going in one direction is the lower limit when travelling in the opposite direction.

The identities in (20) are also of use in computing the points of ill behaviour for $a_{o,o}(a_{o,o}(s))$ and $b_{o,o}(b_{o,o}(s))$. We want to find the points s^* such that $b_{o,o}(b_{o,o}(s))$ is ill behaved in a neighbourhood of s^*. Thus we want to solve $b_{o,o}(s^*) = \sigma$, where σ is a point such that $b_{o,o}(s)$ is ill behaved in a neighbourhood of σ. Solve this by using $s^* = a_{o,o}(\sigma)$. The collection of all such points are indicated in Fig. 6 by '$\diamond$', where the original points $r(s)$ of potential ill behaviour for u are shown by '$\circ$'. Alternatively, let $\mathcal{S}_0$ be the set of corners of Γ, and let $\mathcal{S}_1$ be the union of $\mathcal{S}_0$ and the points of ill behaviour for u as based on its first derivative. To obtain $\mathcal{S}_2$, apply both $a_{o,o}$ and $b_{o,o}$ to $\mathcal{S}_1$. All the new points in $\mathcal{S}_2$ are points at which $a_{o,o} \circ a_{o,o}$ and $b_{o,o} \circ b_{o,o}$ are ill behaved and at which u is usually ill behaved.

To obtain the points of $\mathcal{S}_1$ and $\mathcal{S}_2$ on a physical basis, we start with the corners of Γ_o and Γ_i, the elements of $\mathcal{S}_0$. Connect the elements of $\mathcal{S}_0$ by line segments in all possible ways. Look for those in which the line segment lies entirely within the region bounded by Γ. If such a line segment intersects another point of Γ that is viewable directly from the original points in the line segment, then this is an element of $\mathcal{S}_1$. The elements of $\mathcal{S}_2$ are defined analogously by connecting all of the points of $\mathcal{S}_1$ in the same manner, looking for points of intersection with Γ. This procedure works only if Γ is composed entirely of polygonal paths.

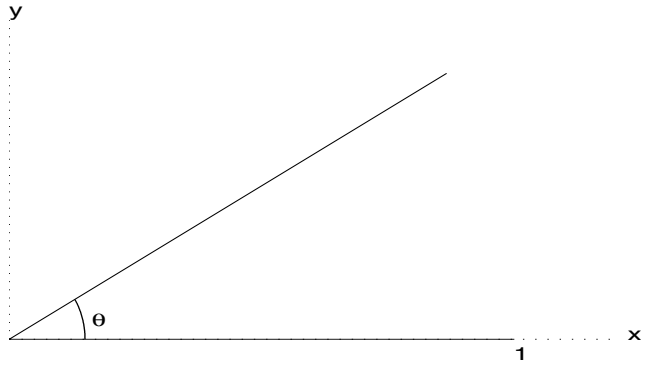

FIG. 7. An unoccluded corner of a polyhedral boundary, with inner angle θ.

We can of course continue this recursively, and doing so we will obtain that the elements of $\mathcal{S}_k - \mathcal{S}_{k-1}$ are new points at which the kth derivative of $u(r(s))$ is likely to be discontinuous. This construction works for all polygonal curves Γ. The curve in Fig. 5 shows that formulas (12)–(13) will need to be generalized, but the same kind of integrals and limits will be involved. We have also omitted the concept of a 'point source'. The latter is popular in the literature, but we prefer to consider such sources as being defined over a small non-empty element.

For curves Γ that are not polygonal, as in Fig. 4, we must generalize the construction. As can be seen from that figure, we must sometimes connect the corner points of Γ_o with points of tangency of Γ_i, in this case with points on $\Gamma_{i,1}$, in order to obtain the elements of $\mathcal{S}_1$. We consider here mainly the case of polygonal curves Γ.

4. Behaviour at corners

The solution of the integral equation (1) has singular behaviour around corner points, much as with the corresponding boundary integral equations of the second kind for solving Laplace's equation on a planar region with corners. Consider the corner shown in Fig. 7, to be called a 'wedge' in this paper. It has both arms of length 1, its vertex is at the origin, and it has a central angle of θ with $0 < \theta < \pi$, with this angular region being included in the domain enclosed by Γ. This restriction is needed in order that the two arms can 'see each other'. We will initially consider the integral equation (1) over this boundary, as the behaviour of the solution in this case is typical of what happens in the case of a general polyhedral boundary. For general boundaries, we would decompose the boundary into ε-neighbourhoods of the corner points and the sections between those points. The regularity properties when using the wedge of Fig. 7 turn out to be the same as when considering an ε-neighbourhood of a corner.

The integral equation (1) on the wedge becomes

$$\begin{aligned} u_1(x) - \frac{\rho_1(x)}{2}\sin^2\theta \int_0^1 \frac{xr\,u_2(r)\,\mathrm{d}r}{\left[x^2+r^2-2xr\cos\theta\right]^{\frac{3}{2}}} &= E_1(x), \\ u_2(x) - \frac{\rho_2(x)}{2}\sin^2\theta \int_0^1 \frac{xr\,u_1(r)\,\mathrm{d}r}{\left[x^2+r^2-2xr\cos\theta\right]^{\frac{3}{2}}} &= E_2(x) \end{aligned} \tag{21}$$

for $0 < x \leqslant 1$ and

$$u_1(x) = u(x,0), \quad u_2(x) = u(x\cos\theta, x\sin\theta)$$

with analogous notation for ρ_1, ρ_2, E_1, E_2. We can prove that if ρ_1, ρ_2, E_1, $E_2 \in C[0,1]$, and if

$$\|\rho\|_\infty = \max\left\{\|\rho_1\|_\infty, \|\rho_2\|_\infty\right\} < 1$$

then u_1 and u_2 exist, are unique, and are continuous on $(0,1]$. Whether or not there is continuity at the origin depends on whether ρ and E are continuous at the origin of the wedge. Moreover, regularity results for u_1 and u_2 on $(0,1]$ follow directly from (21) and the regularity of ρ_1, ρ_2, E_1, E_2. The proofs are omitted.

Assume now that the reflectivities ρ_1 and ρ_2 are nonzero constants, although not necessarily the same. Modify the first equation by dividing by $\sqrt{\rho_1}$ and the second by $\sqrt{\rho_2}$. Introduce new unknowns

$$v_j(x) = \frac{u_j(x)}{\sqrt{\rho_j}}, \qquad j = 1,2$$

and obtain the new equations

$$\begin{aligned} v_1(x) - \frac{\sqrt{\rho_1\rho_2}}{2}\sin^2\theta \int_0^1 \frac{xr\,v_2(r)\,\mathrm{d}r}{\left[x^2+r^2-2xr\cos\theta\right]^{\frac{3}{2}}} &= \frac{E_1(x)}{\sqrt{\rho_1}}, \\ v_2(x) - \frac{\sqrt{\rho_1\rho_2}}{2}\sin^2\theta \int_0^1 \frac{xr\,v_1(r)\,\mathrm{d}r}{\left[x^2+r^2-2xr\cos\theta\right]^{\frac{3}{2}}} &= \frac{E_2(x)}{\sqrt{\rho_2}}. \end{aligned}$$

We add and subtract these equations, obtaining

$$v_\pm(x) \mp \frac{\sqrt{\rho_1\rho_2}}{2}\sin^2\theta \int_0^1 \frac{(x/r)\,v_\pm(r)}{\left[(x/r)^2+1-2\,(x/r)\cos\theta\right]^{\frac{3}{2}}}\,\frac{\mathrm{d}r}{r} = E_\pm(x), \quad 0 < x \leqslant 1$$

with $v_+ = v_1 + v_2$, $v_-(x) = v_1 - v_2$, and similarly for $E_\pm(x)$. These are Mellin convolution integral equations of the second kind, with the Mellin kernel

$$k(t) = \frac{\sqrt{\rho_1\rho_2}}{2}\,\frac{t\sin^2\theta}{\left[t^2-2t\cos\theta+1\right]^{\frac{3}{2}}}, \qquad t \geqslant 0. \tag{22}$$

Using it, we can write the integral equations as

$$v_{\pm}(x) \mp \int_0^1 k\left(\frac{x}{r}\right) v_{\pm}(r)\,\frac{\mathrm{d}r}{r} = E_{\pm}(x), \quad 0 < x \leqslant 1. \tag{23}$$

This reduces the system (21) to the study of two single equations of the second kind in (23), each based on the same integral operator. Letting $x \to 0$, we can also show

$$\begin{aligned}\lim_{x\to 0} \int_0^1 k\left(\frac{x}{r}\right) v(r)\,\frac{\mathrm{d}r}{r} &= v(0)\frac{\sqrt{\rho_1\rho_2}}{2}\int_{-\infty}^{\infty} \frac{\sin^2\theta\, e^{\sigma}\,\mathrm{d}\sigma}{\left[e^{2\sigma} - 2e^{\sigma}\cos\theta + 1\right]^{\frac{3}{2}}} \\ &= \cos^2\left(\frac{\theta}{2}\right)\sqrt{\rho_1\rho_2}\,v(0)\end{aligned} \tag{24}$$

provided $v \in C[0, 1]$. This can be used to calculate the solutions of (23) at $x = 0$:

$$v_{\pm}(0) = \frac{E_{\pm}(0)}{1 \mp \cos^2(\theta/2)\sqrt{\rho_1\rho_2}}.$$

Consider the operator

$$\mathcal{L}v(x) = \begin{cases} \displaystyle\int_0^1 k\left(\frac{x}{r}\right) v(r)\,\frac{\mathrm{d}r}{r}, & 0 < x \leqslant 1, \\ \cos^2\left(\dfrac{\theta}{2}\right)\sqrt{\rho_1\rho_2}\,v(0), & x = 0. \end{cases} \tag{25}$$

This is a bounded operator from $C[0, 1]$ to $C[0, 1]$, with

$$\|\mathcal{L}\| = \cos^2\left(\frac{\theta}{2}\right)\sqrt{\rho_1\rho_2}.$$

For $\rho_1, \rho_2 < 1$, we have that $\|\mathcal{L}\| < 1$, and therefore equation (23) is uniquely solvable in $C[0, 1]$ by the geometric series theorem. Moreover,

$$\|v_{\pm}\|_{\infty} \leqslant \frac{\|E_{\pm}\|_{\infty}}{1 - \|\mathcal{L}\|}. \tag{26}$$

The operator $\mathcal{L}$ is not compact, due to (25) in which it acts like a Dirac delta function.

Integral equations of the form (23) have been well studied in connection with solving planar boundary integral equations for Laplace's equation on polygonal regions in the plane; see, for example, Chandler & Graham (1988), Costabel & Stephan (1985), and Elschner (1990). We can use that framework to study the behaviour of the solutions $v(x)$ to (23) as $x \to 0$. A fundamental result for obtaining this behaviour is the following result taken from Lemma 4.3 of Costabel & Stephan (1985).

LEMMA 3 For a general function w for which $w(\mathrm{e}^{-t})$ belongs to $L^2(-\infty, \infty)$, the Mellin transform $\widehat{w}$ is defined by

$$\widehat{w}(\lambda) = \int_0^{\infty} x^{\mathrm{i}\lambda - 1} w(x)\,\mathrm{d}x = \int_{-\infty}^{\infty} \mathrm{e}^{-\mathrm{i}\lambda t} w(\mathrm{e}^{-t})\,\mathrm{d}t.$$

Assume $\widehat{w}(\lambda)$ is meromorphic in a strip $\text{imag}(\lambda) \in (\alpha_0, \alpha_1 + \varepsilon)$ where $\alpha_0, \alpha_1 \in \mathbb{R}$, $\alpha_0 < \alpha_1$, $\alpha_0 < -\frac{1}{2}$, $\varepsilon > 0$. Assume $\widehat{w}(\lambda)$ has a pole of order 1 at a point ζ for which $\text{imag}(\zeta) = \alpha_1$, and assume there are no other poles in the strip $\alpha_0 < \text{imag}(\lambda) < \alpha_1 + \varepsilon$. For λ in this strip with $\text{imag}(\lambda) = \text{const}$, assume that $\widehat{w}(\lambda)$ is 'rapidly decreasing' as $|\text{real}(\lambda)| \to \infty$. Then

$$w(x) = \gamma\, x^{\alpha_1} + g(x) \tag{27}$$

where $g(x)$ is smoother at $x = 0$ than the function x^{α_1}.

A more precise statement involving membership by w and g in various fractional order Sobolev spaces is given in Lemma 4.3 of Costabel & Stephan (1985).

Consider now the general Mellin convolution integral equation

$$v(x) - \sigma \int_0^\infty k\left(\frac{x}{r}\right) v(r)\, \frac{\mathrm{d}r}{r} = E(x), \quad 0 < x < \infty \tag{28}$$

defined over the entire interval $0 \leqslant x < \infty$, with k an arbitrary Mellin convolution kernel. The constant $\sigma = \pm 1$. Apply the Mellin transform operation to the equation and solve for $\widehat{v}(\lambda)$, obtaining

$$\widehat{v}(\lambda) = \frac{\widehat{E}(\lambda)}{1 - \sigma \widehat{k}(\lambda)}. \tag{29}$$

We determine the zeros of the denominator to locate the poles of $\widehat{v}(\lambda)$. We assume differentiability properties for E and k such that $\widehat{w} \equiv \widehat{v}$ will satisfy the hypotheses of the above lemma. Assuming that $\widehat{E}(\lambda)$ is a well behaved function, we seek the poles of $\widehat{v}(\lambda)$ from the above denominator. We seek a zero ζ of $1 - \sigma \widehat{k}(\lambda)$ for which $\text{imag}(\zeta) = \alpha_1$ with α_1 as small as possible.

Our equation (23) is defined over [0, 1] rather than $[0, \infty)$, but that can be dealt with using standard techniques. To see this, consider the equation

$$v(x) - \sigma \int_0^1 k\left(\frac{x}{r}\right) v(r)\, \frac{\mathrm{d}r}{r} = E(x), \quad 0 < x \leqslant 1. \tag{30}$$

It is a standard construction that we can extend $v(x)$ to all of $[0, \infty)$ in such a way as to preserve whatever smoothness $v(x)$ possesses on (0, 1] and such that support(v) is finite. Having done this, next extend $E(x)$ using

$$E(x) = v(x) - \sigma \int_0^1 k\left(\frac{x}{r}\right) v(r)\, \frac{\mathrm{d}r}{r}, \qquad x > 1.$$

The regularity of E for $x \geqslant 1$ follows from that of k and v. This allows us to now write

$$v(x) - \sigma \int_0^1 k\left(\frac{x}{r}\right) v(r)\, \frac{\mathrm{d}r}{r} = E(x), \quad 0 < x < \infty.$$

Next, add to each side a suitable integral over $[1, \infty)$, to obtain

$$\begin{aligned} v(x) - \sigma \int_0^\infty k\left(\frac{x}{r}\right) v(r)\, \frac{\mathrm{d}r}{r} &= E(x) - \sigma \int_1^\infty k\left(\frac{x}{r}\right) v(r)\, \frac{\mathrm{d}r}{r} \\ &\equiv F(x). \end{aligned}$$

TABLE 1
Exponent values for asymptotic behaviour in (27) for an angle of $\theta = \pi/2$

$\sqrt{\rho_1\rho_2}$	0·1	0·2	0·3	0·4	0·5	0·6	0·7	0·8	0·9	1·0
α_1	0·951	0·903	0·856	0·809	0·763	0·718	0·673	0·627	0·582	0·536

The new function is well defined since $v(r)$ has compact support and the integral is finite; its regularity is easily determined. This new equation is of the desired form (28). Rather than attempting to be general as to the functions k and E to which this argument applies, we will instead consider only the function k of (22) and we assume E is a smooth function on [0, 1]. Then F is an equally smooth function on $[0, \infty)$.

We must now determine whether or not $1 - \sigma\widehat{k}(\lambda)$ has a simple zero ζ with $\text{imag}(\zeta) = \alpha_1$ for some real α_1 and with $1 - \sigma\widehat{k}(\lambda)$ analytic for $\text{imag}(\zeta) < \alpha_1$. This particular problem can be shown to be exactly the same as occurs when examining the edge singularities of the spatial radiosity equation for polyhedral boundaries, and the latter is examined in some detail in Rathsfeld (1997, §2). Separately from us, Rathsfeld notes also that the planar radiosity equation and the spatial radiosity equation with edge singularities reduce to the same Mellin convolution integral equation, although his work is entirely concerned with the more difficult spatial problem.

We apply the results of Rathsfeld (1997, §2) to our situation, and we must examine the denominator $1 - \sigma\widehat{k}(\lambda)$ for the two cases $\sigma = \pm 1$. The case with $\sigma = +1$ leads to smaller values of the exponent α_1 in (27), and thus we consider only that case. Table 1 contains the values of α_1 for an angle of $\theta = \pi/2$, which is the angle in our example in Fig. 2. These results are computed using the Maple code contained in Rathsfeld (1997, §2). As the angle $\theta \to 0$ and the reflectivity $\rho_1\rho_2 \to 1$, it is demonstrated in Rathsfeld (1997, Table 1) that $\alpha_1 \searrow 0$.

These results show that the solutions $u_i(x)$ of (21) will satisfy

$$u_i(x) = c_i x^{\alpha_1} + g_i(x), \qquad i = 1, 2 \tag{31}$$

with $g_i(x)$ having smoother behaviour than x^{α_1}, with α_1 chosen suitably, as in the table. It follows that the first derivative of each $u_i(x)$ will become unbounded as $x \searrow 0$. One consequence is that piecewise polynomial methods of approximating $u_i(x)$ will probably require a graded mesh in order to obtain optimal orders of convergence. We consider this in more detail in §5.

4.1 *The combined effects of corners*

Returning to the radiosity problem posed on the boundary shown in Fig. 2, assume that E is piecewise continuous on $\Gamma = \Gamma_o \cup \Gamma_i$, with E continuous on each polygonal side. Then u will be discontinuous at the corner points of Γ_o and Γ_i, while possessing the behaviour shown in (31). We have in addition that the first derivatives with respect to the arc length of u will be discontinuous at the points indicated by '$\diamond$', '$\square$', and '$\triangle$', with the behaviour of the derivative being a direct consequence of the behaviour of u in the vicinity of the corners of Γ_o. Thus the first derivatives of u will have the behaviour shown in (31) for u around the corner points of Γ_o. This means another form of grading is likely to be needed for the

approximation of u in the neighbourhood of the points $\triangle$ and $\square$, with α_1 in (31) replaced by $\alpha_1 + 1$ at such points. This can be continued to the points at which the second derivative of u is discontinuous, indicated by '$\diamond$' in Fig. 6, with the second derivative having a behaviour as in (31), but with α_1 replaced by $\alpha_1 + 2$ at such points. Clearly we can continue this *ad infinitum*.

5. The collocation solution of the radiosity equation

The collocation method for solving (1) amounts to finding a particular function from a given class so that it satisfies the integral equation at a given set of node points on Γ. We use trial functions which are piecewise polynomial of a given degree $d \geqslant 0$. See Chapter 3 of Atkinson (1997) for a review of the general theory of collocation methods. The collocation method approximates the radiosity $(u \circ r)(s) \equiv u(r(s))$, and this requires knowing the points of discontinuity of the radiosity and its low-order derivatives. Again, we restrict ourselves to boundaries Γ consisting of two parts Γ_o and Γ_i.

We need a set of 'breakpoints' for defining our piecewise polynomial approximation on Γ_o. To begin, let

$$0 = \sigma_0 < \sigma_1 < \cdots < \sigma_\ell = 1 \tag{32}$$

be chosen so that the set $\{r_o(\sigma_i)\}$ contains all the corners of Γ_o. In addition, for interpolation of degree d, assume $\{r_o(\sigma_i)\}$ contains all points at which the derivatives

$$\frac{\mathrm{d}^k}{\mathrm{d}s^k}\left[u(r(s))\right], \qquad k = 1, ..., d$$

are discontinuous. Let a sequence of meshes $\{\mathcal{M}_n \mid n = 1, 2, ...\}$ be given for $[0, 1]$; we write $\mathcal{M}_n$ as

$$0 = t_0^{(n)} < t_1^{(n)} < \cdots < t_{N_n}^{(n)} = 1$$

and assume each $\mathcal{M}_n$ contains the set $\{\sigma_i\}$ of (32). Let

$$h_n = \max_{i=1,...,N_n} \left(t_i^{(n)} - t_{i-1}^{(n)}\right).$$

To simplify the notation, we generally omit the reference to n in $\{t_i^{(n)}\}$ and h_n when the meaning is clear.

Introduce a mesh

$$0 \leqslant \eta_0 < \eta_1 < \cdots < \eta_d \leqslant 1. \tag{33}$$

On each interval $[t_{i-1}, t_i]$, define $d + 1$ interpolation nodes by

$$\tau_{i,j} = t_{i-1} + \eta_j (t_i - t_{i-1}), \qquad j = 0, 1, ..., d. \tag{34}$$

Given $f \in C[0, 1]$, define a piecewise polynomial interpolant of f as follows. For $t_{i-1} < s < t_i$, let $\mathcal{P}_n f(s)$ be the polynomial of degree $\leqslant d$ that interpolates f at the points $\left\{\tau_{i,j} \mid 0 \leqslant j \leqslant d\right\}$. If $\eta_0 = 0$ and $\eta_d = 1$, then the function $\mathcal{P}_n f(s)$ is continuous on

[0, 1]; otherwise, it is discontinuous at the breakpoints in $\mathcal{M}_n$. For the former case, $\mathcal{P}_n$ is a projection on $C[0, 1]$; and in the latter case, it can be extended to be a projection on $L^\infty(0, 1)$, in the same manner as is discussed following Lemma 1. Proceed exactly the same in defining a set of interpolatory node points over Γ_i, and also define $\mathcal{P}_n$ in the same manner. We will use $\mathcal{P}_n$ to refer to the interpolatory approximation over both Γ_o and Γ_i, so long as there is no confusion.

The collocation approximation method for solving (1), $u - \mathcal{K}u = E$, is

$$u_n - \mathcal{P}_n \mathcal{K} u_n = \mathcal{P}_n E. \tag{35}$$

If it is known that $(I - \mathcal{P}_n \mathcal{K})^{-1}$ exists, then the error satisfies

$$u - u_n = (I - \mathcal{P}_n \mathcal{K})^{-1} (I - \mathcal{P}_n) u. \tag{36}$$

For the error in the interpolatory approximation of $u(r(s))$, we need the following lemma and corollary.

LEMMA 4 Let $d \geqslant 0$ be an integer, and assume $v \in C^d[a, b]$ and $v^{(d+1)} \in L^1(a, b)$. Let $d + 1$ nodes be given in [0, 1] as in (33). Define $d + 1$ interpolation nodes on $[a, b]$ by

$$\tau_k = a + \eta_k (b - a), \qquad k = 0, 1, ..., d \tag{37}$$

and let $\mathcal{P}_d v$ denote the polynomial of degree $\leqslant d$ that interpolates v at these nodes. Then

$$\|v - \mathcal{P}_d v\|_\infty \leqslant c_d h^d \left\| v^{(d+1)} \right\|_1 \tag{38}$$

where $h = b - a$.

Proof. This is slightly stronger than the standard interpolation error result which assumes $v \in C^{d+1}[a, b]$. To prove it, use the Peano kernel formulation for the interpolation error to write

$$v(s) - \mathcal{P}_d v(s) = \int_a^b K_d(s, t) v^{(d+1)}(t)\, \mathrm{d}t, \tag{39}$$

$$K_d(s, t) = \frac{1}{d!} \left[p_t(s) - (\mathcal{P}_d p_t)(\sigma) \right],$$

$$p_t(\sigma) = \begin{cases} (\sigma - t)^d, & \sigma \geqslant t, \\ 0, & \sigma < t. \end{cases}$$

If we write $s = a + \xi h$ and use the definition (37), then we can use a change of variables to show

$$v(s) - \mathcal{P}_d v(s) = h^{d+1} \int_0^1 \widetilde{K}_d(\xi, \zeta) v^{(d+1)}(a + \zeta h)\, \mathrm{d}\zeta, \tag{40}$$

$$\widetilde{K}_d(\xi, \zeta) = \frac{1}{d!}\left[p_\zeta(\xi) - \left(\widetilde{\mathcal{P}}_d p_\zeta\right)(\xi)\right],$$

where $\widetilde{\mathcal{P}}_d$ denotes interpolation at the nodes of (33). For a given set of points (33) and for $d > 0$, it is straightforward to see that $\widetilde{K}_d(\xi, \zeta)$ is a continuous function of $\xi, \zeta \in [0, 1]$, and therefore it is bounded on [0, 1], say by a constant c_d. It can be shown directly for $d = 0$ that $\widetilde{K}_d(\xi, \zeta)$ is bounded.

Take absolute values in (40) and use

$$h\int_0^1 \left|v^{(d+1)}(a + \zeta h)\right| \, \mathrm{d}\zeta = \int_a^b \left|v^{(d+1)}(t)\right| \, \mathrm{d}t.$$

This completes the proof of (38). □

COROLLARY 5 Assume $v^{(d+1)}(s)$ exists except on a set of measure zero, say S, and

$$\left\|v^{(d+1)}\right\|_\infty \equiv \sup_{s\in[a,b]\setminus S} \left|v^{(d+1)}(s)\right| < \infty.$$

Then

$$\|v - \mathcal{P}_d v\|_\infty \leqslant c_d h^{d+1} \left\|v^{(d+1)}\right\|_\infty. \tag{41}$$

Proof. Use (38) and

$$\left\|v^{(d+1)}\right\|_1 \leqslant h \left\|v^{(d+1)}\right\|_\infty.$$

□

Using this corollary, and recalling the assumption that $\mathcal{M}_n$ contains the points $\{\sigma_i\}$ as discussed following (32), we can obtain a rate of convergence for $\mathcal{P}_n u$ to u. Assuming $v \equiv u \circ r \in C^d[0, 1]$ for both Γ_o and Γ_i, and assuming $v^{(d+1)}$ is bounded, we obtain

$$\|v - \mathcal{P}_n v\|_\infty \leqslant c_d h^{d+1} \left\|v^{(d+1)}\right\|_\infty. \tag{42}$$

5.1 *Effects due to corners*

Except for the effects examined in §4, the above would be a nearly complete convergence analysis. However, the presence of corners has two consequences. First, the behaviour of u around corner points, given in (27), requires a 'graded mesh' $\{t_i\}$ for $\{r(t_i)\}$ in the vicinity of the corners of Γ in order to accurately approximate u. Second, the integral operator $\mathcal{K}$ is not compact, as noted following (26), making more difficult the demonstration of solvability and stability for (35), i.e. showing existence and uniform boundedness of $(I - \mathcal{P}_n\mathcal{K})^{-1}$ for all sufficiently large n. This stability is needed in (36), to obtain bounds on the rate of convergence.

It was shown in §4 that the operator $\mathcal{K}$ behaves like a Mellin convolution integral operator. A convergence theory for collocation methods of this kind has been given by Chandler & Graham (1988), and we apply their work to the planar radiosity equation. To

do so, we return to the notation of §4. In particular, we look at the use of the collocation method for solving (23),

$$v_{\pm}(x) \mp \int_0^1 k\left(\frac{x}{r}\right) v_{\pm}(r)\,\frac{\mathrm{d}r}{r} = E_{\pm}(x), \quad 0 < x \leqslant 1. \tag{43}$$

We refer to this generically as

$$v - \mathcal{L}v = E \tag{44}$$

with $\mathcal{L}$ a Mellin convolution integral operator. With such Mellin convolution integral equations, we must be more specific as to the meshes $\{t_i\}$.

For a power $q \geqslant 1$ and a mesh parameter m, define a set of breakpoints on [0, 1] by

$$t_i = \left(\frac{i}{m}\right)^q, \qquad i = 0, 1, ..., m. \tag{45}$$

When applied to points of the original boundary Γ, the mesh parameter m will be an approximately fixed fraction of n, the number of subdivisions of Γ. The exponent q is called the 'grading parameter', and as it increases, the nodes $\{t_i\}$ are clustered increasingly around $s = 0$. We proceed as before in defining interpolation nodes, as in (34); we also define the piecewise interpolatory projection operator $\mathcal{P}_m$ as before. Figure 8 illustrates the increased grading of the mesh when q is increased, for $m = 4, 8, 16$. In fact, some of the breakpoints become visually indistinguishable for even such small values of m. Nonetheless, such graded meshes are important in obtaining maximal orders of convergence in our collocation method.

Consider functions $v \in C[0, 1]$ of the form

$$v(s) = v_0 + \alpha(s)\, s^{\gamma}, \qquad s \geqslant 0 \tag{46}$$

with $\gamma > 0$ and $\alpha(s)$ a function with many continuous derivatives on [0, 1], $\alpha(0) \neq 0$. In order to approximate such functions v accurately, we must use a suitably large grading parameter q. A review of results on such 'graded mesh approximations' is given in Atkinson (1997, p 128), and we quote from those results.

Let d and γ be given. Then for $m \geqslant 1$, choose q to satisfy

$$q \geqslant \max\left\{1, \frac{d+1}{\gamma}\right\}. \tag{47}$$

With such a choice,

$$\|v - \mathcal{P}_m v\|_{\infty} \leqslant \frac{c}{m^{d+1}} \tag{48}$$

for some constant c.

The collocation method for solving (44) is

$$v_m - \mathcal{P}_m \mathcal{L} v_m = \mathcal{P}_m E. \tag{49}$$

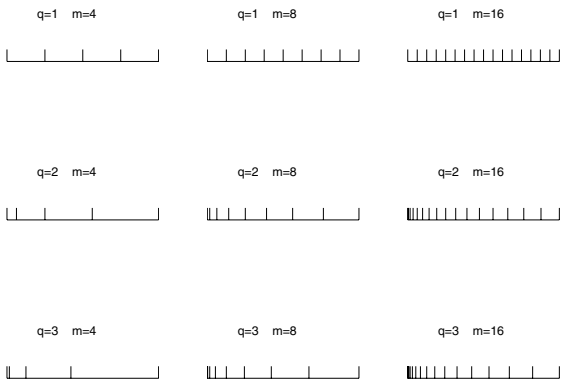

FIG. 8. The graded meshes of (45) for $q = 1, 2, 3$ and $m = 4, 8, 16$.

The stability and convergence analysis of Chandler & Graham (1988) requires a special modification of the interpolatory operator $\mathcal{P}_m$. Let $i^* \geqslant 0$ be given, independent of m. For interpolation of $v \in C[0, 1]$ on the intervals $\left[t_{i-1}, t_i\right]$, $i \leqslant i^*$, define

$$\mathcal{P}_m v(s) = v\left(\tfrac{1}{2}\,(t_{i-1} + t_i)\right), \qquad t_{i-1} < s < t_i. \tag{50}$$

On the remaining subintervals $\left[t_{i-1}, t_i\right]$, define $\mathcal{P}_m v$ as before.

Recall from (31) the exponent α_1. With this exponent $\gamma = \alpha_1$, the Mellin operator $\mathcal{L}$ can be shown to satisfy the hypotheses of Chandler & Graham (1988, Thm 6) when the grading parameter q satisfies (47). It follows from Chandler & Graham (1988, Thm 6) that there is some $i^* \geqslant 0$ for which $(I - \mathcal{P}_m\mathcal{L})^{-1}$ exists and is uniformly bounded for all sufficiently large m, say $m \geqslant m_0$. Moreover,

$$\|v - v_m\|_\infty \leqslant \frac{c}{m^{d+1}}, \qquad m \geqslant m_0 \tag{51}$$

for some constant $c > 0$. It is not known how to choose i^*, so one usually starts with $i^* = 0$ and see if that works (and it usually does).

5.2 *Defining the breakpoints*

If $r(s)$ is a corner of Γ, then the mesh needs to be defined according to the above with the choice of $\gamma = \alpha_1$ for that corner. Next, suppose one is at a point $r(s^*)$ at which

$$\frac{\mathrm{d}}{\mathrm{d}s}\left[u(r(s))\right]$$

is discontinuous due to $r(a_{o,o}(s^*))$, $r(b_{o,o}(s^*))$, or some other analogous point being a corner of Γ (as explored earlier in §3). Then $u(r(s))$ will have a behaviour (46) with

$\gamma = \alpha_1 + 1$, with α_1 associated with the corner in question. Then the mesh needs to be graded about such a point s^* to reflect this behaviour in the solution $u(r(s))$. Such points are illustrated in Fig. 2 with the symbols '$\square$', '$\diamond$', and '$\triangle$'. This continues to the other points s at which the higher derivatives

$$\frac{\mathrm{d}^k}{\mathrm{d}s^k}\left[u(r(s))\right], \qquad k = 1, ..., d$$

are discontinuous, with correspondingly higher values of $\gamma = \alpha_1 + k$. Our numerical examples are for collocation with piecewise constant functions, implying $d = 0$, and we consider as *singular points* only those points s at which $u(r(s))$ or its first derivative are discontinuous.

We now describe approximately our method for defining the mesh for dividing a curve C, say Γ_o or Γ_i. We choose an integer n_C which will be doubled successively to obtain increasing accuracy. Let $s = \alpha$ and $s = \beta$ correspond to successive points of possible singularity in $u(r(s))$ on C, say corresponding to the points of discontinuity of $[u(r(s))]'$ illustrated in Fig. 2. Then we assign the number of breakpoint subdivisions of $[\alpha, \beta]$ to be approximately

$$(\beta - \alpha)\frac{n_C}{|C|}$$

where the length of C is denoted by $|C|$, with a minimum of 4 such subdivisions in every case. We let n denote the total number of mesh subdivisions for all parts of Γ. This mesh will be graded in accordance with (45) and (47).

5.3 *Superconvergence*

In Chandler & Graham (1988, Thm 6), it is also demonstrated that superconvergence results are possible at the collocation node points. Assume the mesh grading parameter is chosen sufficiently large,

$$q > \max\left\{1, \frac{2(d+1)}{\gamma}\right\}. \tag{52}$$

Also, let the points $\{\eta_j\}$ of (33) be chosen as the Gauss–Legendre zeros of order $d + 1$ relative to $[0, 1]$. Then the result (51) can be improved to

$$\max_{\tau_{i,j}} \left|v(\tau_{i,j}) - v_m(\tau_{i,j})\right| \leqslant \frac{c}{m^{2(d+1)}}, \qquad m \geqslant m_0 \tag{53}$$

for the error at the collocation node points of (34).

For the case of $d = 0$, the superconvergent collocation method is simply based on piecewise constant interpolation at the midpoint of each subinterval $[t_{i-1}, t_i]$. The condition (52) becomes

$$q > \max\left\{1, \frac{2}{\gamma}\right\}. \tag{54}$$

This is illustrated in the next section. The convergence results of (51) and (53) are respectively

$$\|v - v_m\|_\infty \leqslant \frac{c}{m}, \qquad m \geqslant m_0, \tag{55}$$

$$\mathcal{E}_m \equiv \max_{\tau_j} \left|v(\tau_{i,j}) - v_m(\tau_{i,j})\right| \leqslant \frac{c}{m^2}, \qquad m \geqslant m_0. \tag{56}$$

The result (55) could have been proven directly without the theory of Chandler & Graham (1988, Thm 6). The stability of the numerical method follows easily, as $\|\mathcal{P}_m\| = 1$ and therefore

$$\begin{aligned} \|\mathcal{P}_m\mathcal{K}\| &\leqslant \|\mathcal{K}\| \\ &\leqslant \|\rho\|_\infty < 1. \end{aligned}$$

The geometric series theorem then implies the stability result

$$\left\| (I - \mathcal{P}_m\mathcal{K})^{-1} \right\|_\infty \leqslant \frac{1}{1 - \|\mathcal{K}\|}.$$

The convergence result (55) is then straightforward from (36), provided that the mesh is sufficiently graded relative to the regularity of the radiosity solution. But the improved superconvergence result (56) requires the results of Chandler & Graham (1988, Thm 6).

6. Numerical examples

All of our numerical examples are for the boundary Γ of Fig. 2, and the collocation integrals are all evaluated analytically, to give the exact integrals in all cases. For all cases, we defined the inner boundary using $a = 0{\cdot}5$, and for the reflectivity, we used $\rho(P) \equiv 0{\cdot}9$, over both Γ_o and Γ_i. We begin with an illustration of the possible behaviour of the radiosity solution. Define the emissivity function by

$$E(x, y) = \begin{cases} 2 + x + y, & (x, y) \in \Gamma_o, \\ 0, & (x, y) \in \Gamma_i. \end{cases} \tag{57}$$

The resulting radiosity over Γ_o is shown in Fig. 9.

Note first the discontinuities at $s = \frac{1}{4}, \frac{3}{4}$, corresponding to the corners of Γ_o at $(-1, 1)$ and $(1, -1)$. There are no discontinuities at the other two corners due to symmetry considerations. Recall that the continuity of $u(r_o(s))$ was discussed in the second paragraph of §3.1. Also in Fig. 9, there appear to be power singularities at $s = 0$ and $\frac{1}{2}$.

As a second example, define the emissivity by

$$E(r_i(s)) \equiv 0, \qquad E(r_o(s)) = \begin{cases} 25s\left(\frac{1}{4} - s\right), & 0 \leqslant s \leqslant \frac{1}{4}, \\ 0, & \frac{1}{4} \leqslant s \leqslant 1. \end{cases} \tag{58}$$

Thus only the top edge of Fig. 2 shows any emission of light; and the emissivity is continuous over Γ. The resulting radiosity over Γ_o is shown in Fig. 10. With reference

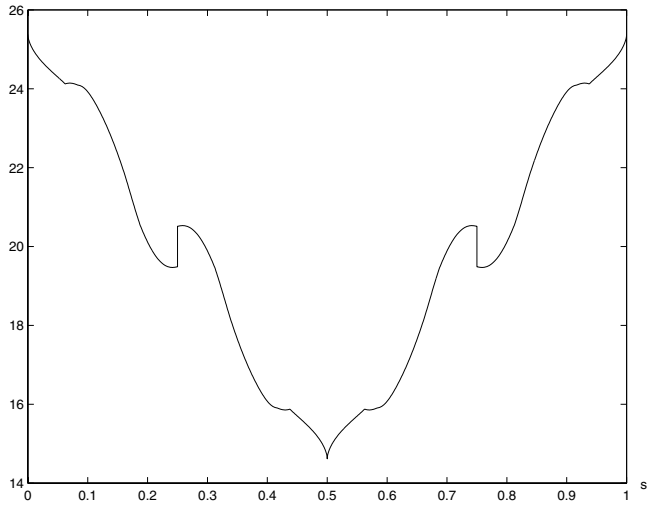

FIG. 9. Radiosity for emissivity $E = 2 + x + y$ on Γ_o, with $a = 0{\cdot}5$ and $\rho \equiv 0{\cdot}9$.

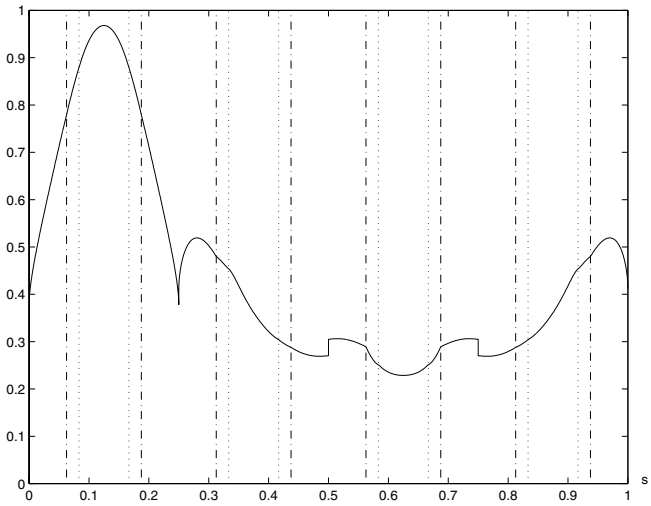

FIG. 10. Radiosity for emissivity of (58), with $a = 0{\cdot}5$ and $\rho \equiv 0{\cdot}9$.

to Fig. 2, the points '$\diamond$' and '$\square$' are indicated by the dotted vertical lines, and the points '$\triangle$' are indicated by the chain vertical lines.

Note the discontinuities at $s = \frac{1}{2}, \frac{3}{4}$, and that there appear to be discontinuities in $(u(r_o(s)))'$ at other points. The solution $u(r_o(s))$ appears to have a power-type singularity, as in (46), at $s = \frac{1}{4} + 0$ and $s = 1 - 0$, meaning to the right of $s = \frac{1}{4}$ and to the left of

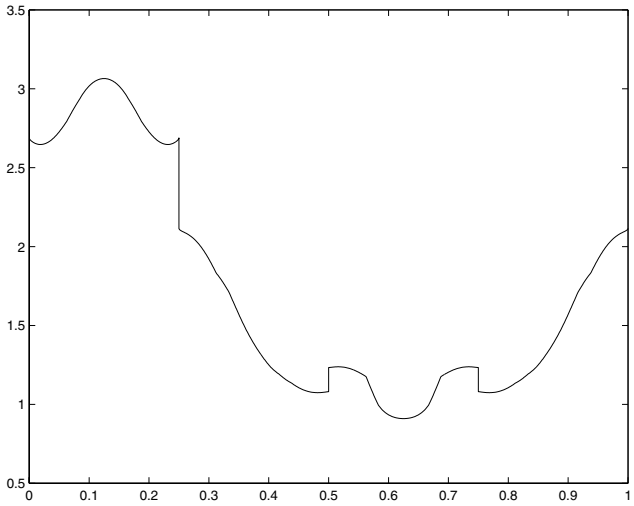

FIG. 11. Radiosity for emissivity of (59), with $a = 0{\cdot}5$ and $\rho \equiv 0{\cdot}9$.

$s = 1$. Using an empirical fit to the data, the power singularity appears to have the form

$$u(r_o(s)) \approx 0{\cdot}412 + 1{\cdot}331\left(s - \tfrac{1}{4}\right)^{0{\cdot}588}, \qquad s > \tfrac{1}{4}$$

with s close to $\frac{1}{4}$. Note the close agreement to the exponent value given in Table 1. There are clear discontinuities in $(u(r_o(s)))'$ at the points $s = 0{\cdot}5625, 0{\cdot}6875$, which are points denoted '$\triangle$' in Fig. 2. Visually, it appears that the derivative is also discontinuous at other points as well, including at some points of type '$\diamond$' and '$\square$'.

A third example is given in Fig. 11 for the emissivity

$$E(r_i(s)) \equiv 0, \qquad E(r_o(s)) = \begin{cases} 1, & 0 \leqslant s \leqslant \frac{1}{4}, \\ 0, & \frac{1}{4} \leqslant s \leqslant 1. \end{cases} \tag{59}$$

Our numerical examples are just for the midpoint collocation method using piecewise constant functions, discussed at the end of §5. We begin with the case of a known radiosity solution,

$$u(x, y) = 2 + x + y,$$

with the emissivity $E = u - \mathcal{K}u$ and $\mathcal{K}u$ produced by analytical integration. Table 2 contains results for varying values of the grading parameter q. With a right angle, the value of $\gamma = 0{\cdot}582$ is the likely singularity in the power singularity of (46) for most radiosity solutions, although in the present case we have a smooth solution. In Table 2, n_o and n_i are the number of breakpoint subdivisions of Γ_o and Γ_i, respectively, and $n = n_o + n_i$ is the order of the linear system associated with the collocation method. The linear system was solved directly using Gaussian elimination. The quantity labeled *EOC* denotes the

TABLE 2
Rates of convergence

		$\mathcal{E}_n$					
n_o	n_i	$q = 1$	EOC	$q = \frac{3}{2}$	EOC	$q = 2$	EOC
88	16	1·087E−2		1·326E−2		1·643E−2	
168	32	3·051E−3	1·83	3·700E−3	1·84	4·406E−3	2·02
320	64	1·000E−3	1·61	1·130E−3	1·71	1·109E−3	1·99
648	128	3·634E−4	1·46	3·483E−4	1·70	2·882E−4	1·94
1280	256	1·487E−4	1·29	1·104E−4	1·66	7·344E−5	1·97

'estimated order of convergence'. In our case, since we are approximately doubling n, we use

$$EOC = \frac{\log \mathcal{E}_n - \log \mathcal{E}_{2n}}{\log 2}.$$

Based on (56), we would like to have $EOC \doteq 2{\cdot}0$.

A more accurate estimate can be found by comparing $\log n$ to $\log \mathcal{E}_n$. In the plots of $\log n$ versus $\log \mathcal{E}_n$ for the data of the table, both of the cases $q = \frac{3}{2}$ and $q = 2$ show a strong linear relationship, meaning

$$\mathcal{E}_n \doteq c_q n^{-p_q}.$$

Using this linear relationship for the cases $q = \frac{3}{2}$ and $q = 2$, the respective limiting values of p_q appear to be approximately 1·68 and 2·00. For $q = 1$, a limiting behaviour is not apparent, but we hypothesize that $p_1 \doteq 1$ for sufficiently large values of n.

6.1 *Interpolation of the collocation solution*

Assuming we have used a properly graded mesh, we have second-order convergence of (56). In extending the solution to other points, what form of interpolation should be used? We have used linear interpolation of the collocation solution, but without interpolating across the corner points of the boundary. When very near to a corner, say at $s = s^*$ near to a corner parameter, choose the two collocation points nearest to s^* that are on the same side of the corner as s^*. Again use linear interpolation based on these two collocation points, extrapolating to obtain the value at s^*. We chose approximately 4000 uniformly spaced points in [0, 1], interpolating at these points the collocation solutions for

$$n_o = (88, 168, 320, 648, 1280), \qquad n_i = (16, 32, 64, 128, 256)$$

and $n = n_o + n_i$. We then differenced successive interpolated solutions, calculating $u_{n_2} - u_{n_1}$ with $n_1 < n_2$ denoting successive values of n. This gives some sense of the error in the computed solutions.

We present results for the radiosity solution with emissivity (58). In Fig. 12, we show the difference $u_{n_2} - u_{n_1}$ of the interpolated solutions for the cases $n_1 = 776$ and $n_2 = 1536$,

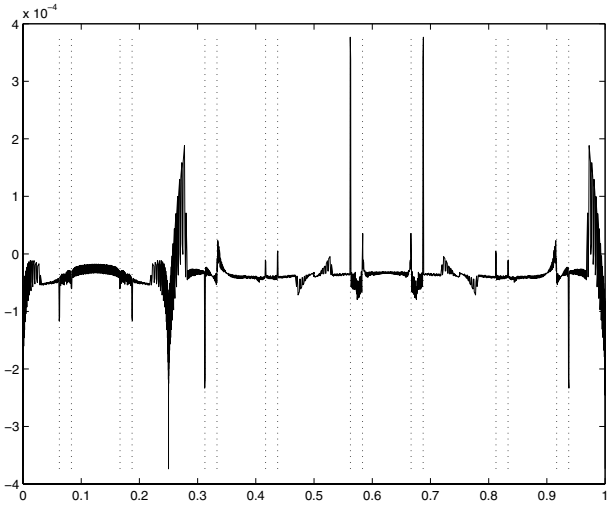

FIG. 12. Difference of interpolated solutions for emissivity (58).

TABLE 3
Norms of differences of successive interpolated solutions

	M_n					
n	$q = 1$	EOC	$q = 2$	EOC	$q = \frac{10}{3}$	EOC
200	2·80E−2		3·01E−2		3·41E−2	
384	1·05E−2	1·4	6·46E−3	2·2	5·49E−3	2·63
776	6·04E−3	0·8	8·67E−4	2·9	1·46E−3	1·91
1536	3·43E−3	0·8	3·87E−4	1·2	3·77E−4	1·95

with grading parameter $q = 2$ around each corner. We have also included the vertical lines given earlier in Fig. 10, marking the points of possible discontinuity in the first derivative of the radiosity solution. Note the occasionally much larger values of the difference function. These occur at corner points and at the points noted by the dotted vertical lines. The error at the power singularity is especially large, indicating that linear interpolation should not be used for such functions. Clearly a better form of interpolation is needed around all such points.

In Table 3 we give the maximums of these differences for various values of q. For notation, we use

$$M_n = \left\| u_n - u_{\frac{1}{2}n} \right\|_\infty$$

based on the differences at the 4000 interpolated values of the computed radiosity solutions. The use of a graded mesh does improve the rate of convergence, but the rate is still not all that good. The reason is due to our use of linear interpolation. As is indicated by Fig. 12,

the error at most points is much smaller than that suggested by the values in Table 3. Consistent with (54), we include the choice of $q = \frac{10}{3}$. Empirically, we have an order of convergence consistent with the theoretically desirable rate of $O(n^{-2})$ of (56).

Acknowledgements

The author thanks Ezio Venturino for talks about the planar radiosity equation in the early stages of this research. I am also indebted to Andreas Rathsfeld and thank him for helping me to obtain an improved understanding of the use and utility of the Mellin transform, especially as used in Lemma 3. This research was supported in part by NSF grant DMS-9403589.

REFERENCES

ATKINSON, K. 1997 *The Numerical Solution of Integral Equations of the Second Kind*. Cambridge: Cambridge University Press.

ATKINSON, K. & CHANDLER, G. 1998 The collocation method for solving the radiosity equation for unoccluded surfaces. *J. Integral Equations Applic.* **10**, 253–290.

ATKINSON, K., GRAHAM, I., & SLOAN, I. 1983 Piecewise continuous collocation for integral equations. *SIAM J. Numer. Anal*. **20**, 172–186.

CHANDLER, G. & GRAHAM, I. 1988 Product integration-collocation methods for non-compact integral operator equations. *Math. Comput.* **50**, 125–138.

COHEN, M. & WALLACE, J. 1993 *Radiosity and Realistic Image Synthesis*. New York: Academic.

COSTABEL, M. & STEPHAN, E. 1985 Boundary integral equations for mixed boundary value problems in polygonal domains and Galerkin approximation. *Mathematical Models and Methods in Mechanics*, Banach Center Publications **15**, Warsaw, pp 175–251.

ELSCHNER, J. 1990 On spline approximation for a class of non-compact integral equations. *Math. Nachr.* **146**, 271–321.

HECKBERT, P. 1991 Simulating global illumination using adaptive meshing. *PhD Thesis*, University of California at Berkeley.

HECKBERT, P. 1992 Radiosity in flatland. *Computer Graphics Forum* **11**, 181–192, *Proceedings of Eurographics '92.*

LISCHINSKI, D., TAMPIERI, F., & GREENBERG, D. 1992 Discontinuity meshing for accurate radiosity. *IEEE Comput. Graphics Applic.* **12**, 25–39.

MODEST, M. 1993 *Radiative Heat Transfer*. New York: McGraw-Hill.

ORTI, R., RIVIERE, S., DURAND, F., & PUECH, C. 1996 Radiosity for dynamic scenes in flatland with the visibility complex. *Eurographics '96*, ed J. Rossignac and F. Sillion. Blackwell Publications, vol. 15, No 3, pp C237–C248.

RATHSFELD, A. 1997 Edge asymptotics for the radiosity equation over polyhedral boundaries. *Preprint 369*, Weierstraß-Institut für Angewandte Analysis und Stochastik, Berlin.

SILLION, F. & PUECH, C. 1994 *Radiosity and Global Illumination*. San Francisco: Morgan Kaufmann.